Chinese Journal of Oceanology and Limnology
Vol. 28 No. 5, P. 1102-1111, 2010
DOI: 10.1007/s00343-010-0146-4

Mesoscale structure of the central South China Sea detected by SCSMEX Buoy and Argo float*

ZENG Lili (曾丽丽) [1], WANG Dongxiao (王东晓) [1], DU Yan (杜岩) [1,**], SHI Ping (施平) [1, 2]

[1] *Key Laboratory of Tropical Marine Environmental Dynamics, South China Sea Institute of Oceanology, Chinese Academy of Sciences, Guangzhou 510301, China*

[2] *Yantai Institute of Coastal Zone Research, Chinese Academy of Sciences, Yantai 264003, China*

Received May 10, 2010; revision accepted July 3, 2010

© Chinese Society for Oceanology and Limnology, Science Press, and Springer-Verlag Berlin Heidelberg 2010

Abstract We addressed the mesoscale structure variation of the central South China Sea (SCS) with the measurements by a long-lived Argo float and a high-resolution ATLAS buoy during 1998–2002. T-S diagram indicates cooling and freshening events in 2000 and 2001 with lower salinity (0.5–0.8) and lower temperature (1–1.7°C). Significant decrease in the net heat flux and increase in the precipitation suggest that the cooling and freshening is due to extra forcing by the atmosphere. Additional to large year-to-year changes, intraseasonal variability is moderate in the research area. The axis of the maximum intraseasonal temperature and salinity signals are mainly located on the thermocline. Typically, amplitude and period of intraseasonal temperature is about 2°C and 40–60 days, and that of salinity is 0.3–0.5 and 35–60 days. Rapidly-changing winds, heat flux, and precipitation are critical in controlling the intraseasonal fluctuations of the mixed layer of the area. Studies on heat and freshwater balance in the mixed-layer further suggest that horizontal advection plays an important role in intraseasonal fluctuation in the upper ocean. In addition, the energetic mesoscale propagation radiated from the east boundary is linked to the intraseasonal variability in winter.

Keyword: South China Sea (SCS); upper ocean; water mass; Argo floats; SCSMEX buoy

1 INTRODUCTION

The South China Sea (SCS) is a semi-enclosed basin with depths of 3 000–4 000 m in the central basin and less than 200 m over most of the peripheral shelves (Fig.1). As a part of the Indo-Pacific warm pool, the SCS is an important part of the Asian monsoon system. It is subject to the strong forcing of alternating northeast and southwest monsoon winds, frequent typhoons, seasonal incursions of the Kuroshio Current, and fresh water inflows from rivers (Xue et al., 2004; Liu et al., 2000). The climate of the basin fluctuates significantly in time scales ranging from intraseasonal to decadal (Liu et al., 2001; Xie et al., 2007a, b).

The upper ocean records mixing events and restratification, as well as the traces of all physical processes occurring above the permanent thermocline (Holte et al., 2009). However, few observations provide data satisfactory for quantifying and improving our understanding of the features of the upper SCS. Observations longer than one year are only available from three ATLAS buoys deployed in the South China Sea Monsoon Experiment (SCSMEX). Our knowledge of the evolution of the upper water masses in the SCS is still limited.

As a part of the successful implementation of the international Argo project, 3 000 profiling floats are deployed to build a real-time monitoring system of the upper and middle layers of the world's oceans since 2000. The Argo floats provide a better monitoring tool than any previous ones and enhance our understanding of the mixing layer and the vertical structures of temperature and salinity (Liu

* Supported by the Knowledge Innovation Program of the Chinese Academy of Sciences (Nos. KZCX1-YW-12-01, KZCX2-YW-BR-04), and the Knowledge Innovation Program of the Chinese Academy of Sciences (Nos. SQ200916, SQ200809), the National Natural Science Foundation of China (No. 40806003), and the National High Technology Research and Development Program of China (863 Program) (No. 2008AA09A402)

** Corresponding author: duyan@scsio.ac.cn

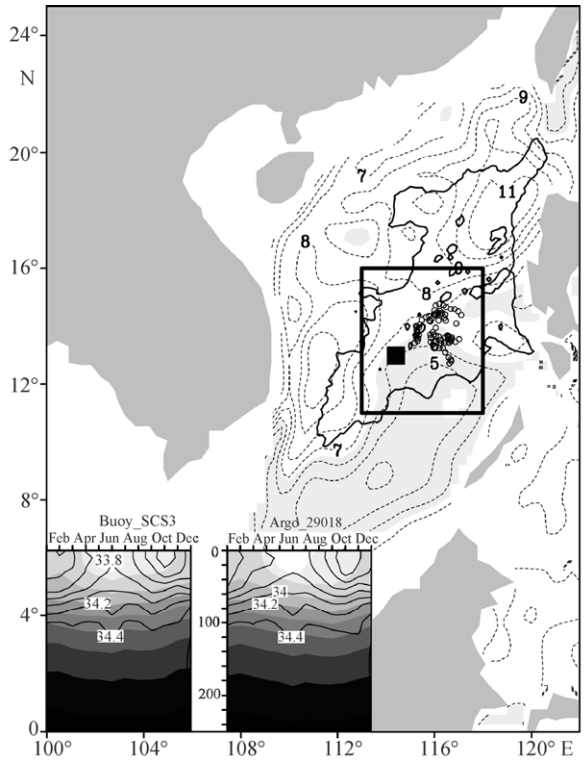

Fig.1 Location of the SCSMEX Buoy_SCS3 (black square) and trajectories of the surface drifter of Argo_29018 (black circles; solid circles are summer measurements)

The 3 500 m isobaths (solid lines) and the standard deviation of climatology sea-level anomaly (1998–2007, shading and dashed contours) are given. The rectangular box (113–118°E, 11–16°N) indicates the main area in the study. The time-depth sections of the temperature (shading) and salinity (contour) from WOA05 at the locations of Buoy_SCS3 and Argo_29018 are given in the left corner

et al., 2007; Su et al., 2008). For the first time, we are able to continuously monitor temperature, salinity, and velocity, have all real-time data relayed, and make these data publicly available within hours after collection (Argo Science Team, 2000, 2001, 2002). Argo floats have been used in studying variations in the mixed layer (Ohno et al., 2004; Sato et al., 2004), the upper ocean response to tropical cyclones (Liu et al., 2007), and water mass formation and variation (Wong et al., 2003; Oka et al., 2003; Oka, 2005).

In this study, we examined the upper ocean variations through observational analysis of data obtained from a moored buoy and an Argo float in the central SCS. It is organized in the following manner. Section 2 describes briefly the observation data and processing procedure. Section 3 presents seasonal and year-to-year changes. Section 4 describes the intraseasonal variability of the upper SCS. Section 5 is a discussion and results are summarized in Section 6.

2 DATA AND METHODS

2.1 Argo float

Twenty seven Argo floats were deployed in the SCS 2000–2008. Data were collected and available to the public by the International Argo Project and Coriolis Project (ftp://ftp.ifremer.fr/ifremer/argo; accessed on 2010/5/10). Although the sampling depths are not uniform, most profiles consisted of about 70 levels in depth of 5–2000 m. At the time of recoverage, Argo_29018 operated for more than 2 years in the central SCS, and provided a precious set oflong-period records sufficiently for examining long-term water masses. The initial location of Argo_29018 was 116.4°E and 13.4°N, and the operational period was from January 20, 2000 to March 29, 2002 (recordings were made in a 7-day interval). The float provides 86 temperature/salinity profiles after quality control. To further check the quality of data collected by Argo_29018, data from Argo_29018 and the World Ocean Database 2009 (WOD09) for waters within the main area in the study (113–118°E, 11–16°N) were compared, and we found that the water properties recorded by Argo floats are reliable (Fig.3).

2.2 SCSMEX buoy

During the SCSMEX, three ATLAS anchored buoys were deployed in the northern central SCS (SCS1), central SCS (SCS2), and southern central SCS (SCS3) to observe sea surface meteorological parameters, ocean temperature, salinity, and current (Liu et al., 2001). The sampling intervals were 10 min. Measurements from the southern moored buoy of the SCSMEX (Buoy_SCS3) were used, located at 12.98°N/114.41°E, from April 20, 1998 to April 8, 1999. The vertical temperature at 1, 25, 50, 75, 100, 125, 150, 200, 250, 300, and 500 m and salinity at 1, 25, 50, and 100 m were recorded. The data was averaged to daily mean data to suppress synoptic disturbances. The location and general information of Argo_29018 and Buoy_SCS3 are given in Table 1 and Fig.1.

2.3 Other in-situ observation

Shipboard conductivity-temperature-depth (CTD) data from a cruise during summer 2000 were used. The cruise took place from August 2 to September 3, 2000 as a joint operation under the support of the National Basic Research Program (973 Program) of China. Temperature and salinity were obtained from the surface to 2 364 m and most data were taken in

Table 1 General information on an Argo float and SCSMEX buoy in the South China Sea used in the study

Buoy & ARGO floats	Initial location	Time period	Time interval	N of TS-profiles
ARGO_29018	116.4°E, 13.4°N	2000/1/20–2002/3/29	7days	86
Buoy_SCS3	114.41°E, 12.98°N	1998/4/12–1999/4/11	10mins	52 278

the deep ocean basin. After quality control procedures set by Qu et al. (2005), the final dataset included 189 profiles in 1-m vertical interval. Monthly climatological temperature and salinity from the World Ocean Atlas 2005 (WOA05) were also used for comparison.

2.4 Satellite measurement

A set of satellite measurements were used, including daily and monthly mean net heat flux taken from the Objective Analysis Flux (OAFlux; Yu et al., 2007) provided by the Woods Hole Oceanographic Institution, daily and monthly mean net fresh water fluxes from the Tropical Rainfall Measuring Mission (TRMM) 3B43-V6 precipitation product (Huffman et al., 2007), satellite-derived evaporation (Zeng et al., 2009a), daily and monthly mean wind speeds from the Special Sensor Microwave Imager (SSM/I; Wentz, 1997), and weekly and monthly merged sea-level anomaly data distributed by AVISO (Volkov et al., 2007).

2.5 Near-surface heat and freshwater balance

Commonly, the variability of the mixed-layer temperature is controlled by

$$\rho C_p H_0\ (\partial SST/\partial t)=Q_{\text{eff}}+Advection+Mixing \qquad (1)$$

where H_0 is the mixed-layer depth and ρ and C_p are the density and specific heat of seawater, respectively. The mixed-layer temperature is $SST=(\int_0^{H_0}T(z)\mathrm{d}z)/H_0$. The heat flux absorbed in the mixed layer (i.e., the effective heat flux (Q_{eff})) is equal to the net surface heat flux minus penetrative shortwave radiation (Q_{open}) below depth H_0. Q_{open} is estimated follow Morel (1988) and Parampil et al. (2010).

The mixed layer freshwater balance is

$$\partial FW/\partial t=P-E+Advection+Mixing \qquad (2)$$

where the freshwater content of the mixed layer is defined as $FW=\int_0^{H_0}((S_{\text{ref}}-S(z))/S_{\text{ref}})\mathrm{d}z$, and the reference salinity is S_{ref} = 34. Net fresh water flux ($P–E$) is precipitation minus evaporation. Limited by data acquirement, we had no estimates of advection or mixing across the base of the mixed layer.

3 SEASONAL AND YEAR-TO-YEAR CHANGES

In the SCS, few long-term observations could be used to investigate the variation of water mass property. Checking the Argo floats deployed in the SCS, it is found that Argo_29018 operated for two years and three months. This Argo float lingered in a small domain (115.18–117.11°E, 12.71–14.77°N) throughout its operation, acting as a "stationary" CTD mooring system, due possibly to weak circulation in the region. As shown in Fig.1, standard deviation of the climatological sea-level anomaly (1998–2007) was low in the southeastern SCS and high west of the Luzon Strait and southeast of Vietnam. The location of Argo_29018 was close to the area of minimum standard deviation. Variance analysis of the high-frequency variability of the sea-level anomaly shows similar characteristics (Zhuang et al., 2010). Therefore, Argo_29018 was regarded as a long-term fixed station if we ignore secondary small spatial changes during observation period. Mooring Buoy_SCS3 (12.98°N, 114.41°E) located near the Argo floats. Comparing with WOA05 (subfigures of Fig.1), the vertical structures at the two locations ware almost the same. Therefore, we use them together to co-validate and investigate the characteristics of water mass in different time scales from 1998 to 2002.

3.1 Seasonal variation

The vertical distributions of temperature and salinity are shown in Fig.2. The isothermal-layer depth and mixed-layer depth are given in the time-depth sections. The depth properties are first derived from individual profiles using the same criteria as Zeng et al. (2009b). The isothermal-layer depth is defined in terms of a temperature step (ΔT = 0.8°C) from near-surface temperature at 10 m, and the mixed-layer depth in terms of a variable density step ($\Delta\rho$), equivalent to ΔT, from the near-surface density. It is seen that the upper-ocean properties have significant seasonal and interannual variation.

A brief description of the seasonal variation is given below.

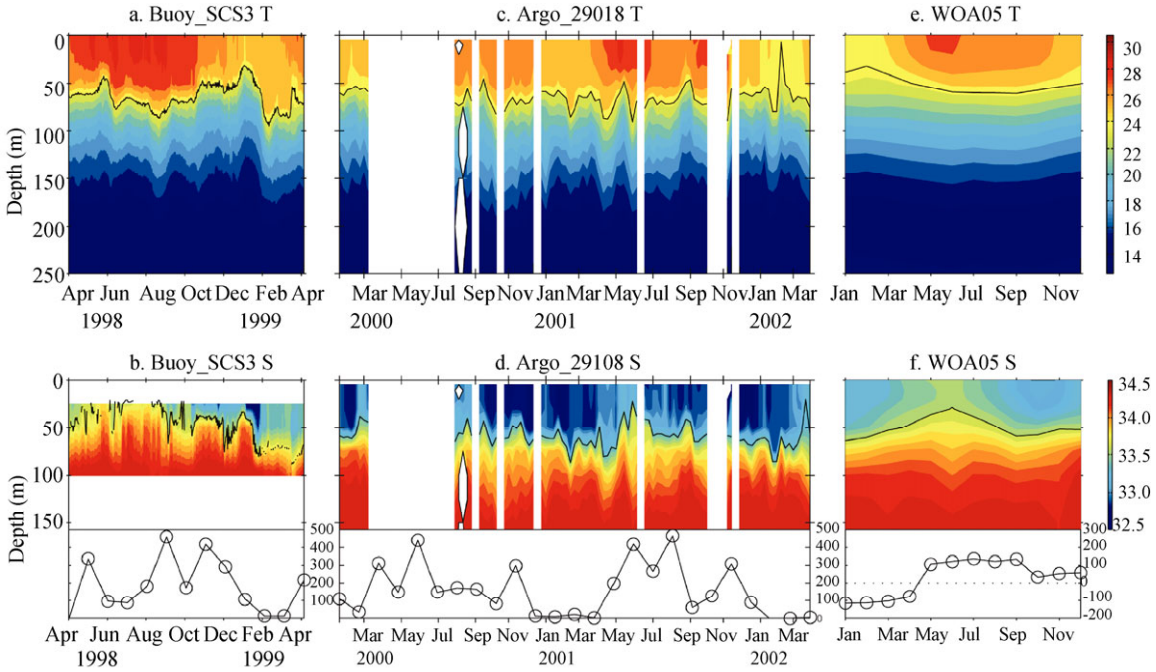

Fig.2 Time-depth sections of the temperature and salinity based on the SCSMEX Buoy_SCS3 (left, a, b), Argo_29018 (middle, c, d) and WOA05 (right, e, f, averaged in the rectangular box marked in Fig.1) measurements

Solid lines show time variations of the depths of the isothermal layer and mixed layer. Monthly precipitation averaged in the marked box in Fig. 1 is given in lower parts of b, d, f, accordingly

3.2 Year-to-year variation

To study the year-to-year changes in the study area, water properties observed in different years are shown in a T-S diagram (Fig.3). The diagram indicates that the upper water masses had large changes from 1998 to 2002. The water in the El Niño year 1998 was much warmer than that in other years, especially that in the La Nina year 1999. This difference illustrates the important influence of the ENSO over the region. Water in 2000, 2001 and 2002 were much colder and fresher than that in 1998. Differences among the three years are relatively small.

Now a question arrives: Were the large interannual changes that recorded by the buoy and Argo float caused by different instruments employed in different periods? The uncertainty of Argo float measurements should be excluded first, as CTD data were used to validate the Argo and buoy observations carried out during summer 2000. As shown in Fig.3, the CTD data indicate cold and fresh water similar to that detected by Argo floats. In other words, the large year-to-year change observed in this area is real and natural. The interannual differences were induced by summer water masses in 1998, and 2000/2001, which was found in our detailed examination. To show the interannual temperature and salinity differences more clearly, a T-S diagram of water masses in summer 1998 obtained from Buoy_SCS3 and summer 2001/2002 obtained from Argo_29018

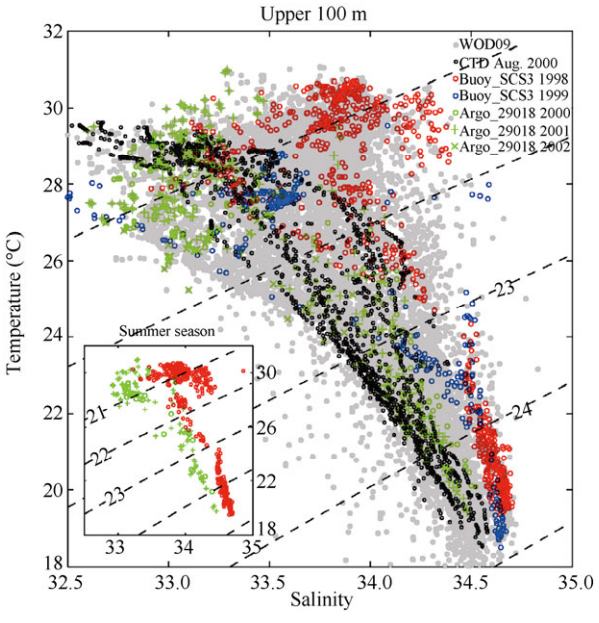

Fig.3 T-S diagram of the upper layer ocean (above 100 m) observed by Buoy_SCS3 and Argo_29018 in different years. Observations from a summer 2000 cruise and WOD09 dataset are also given in the rectangular box Water masses in summer 1998 from Buoy_SCS3 and summer 2001 and 2002 from Argo_29018 are given in the left corner

is presented in the subfigure of Fig.3. The maxima and minima of the temperature and salinity at 25 m are given in Table 2. The maximum and minimum temperatures are 30.7°C and 29.2°C in summer 1998, 29.0°C and 28.2°C in 2000, and 30.9°C and 28.0°C in 2001. Thus, the year-to-year temperature variation among the maxima/minima in 1998 and 2000/2001 is 1.7°C/ 0.8°C. The result of the mean temperature confirms our finding of the maximum/minimum temperature.

We know that the upper ocean variability reflects mainly the interaction between ocean and atmosphere. The year-to-year changes of surface flux are shown in Fig.4 based on the net heat flux obtained from OAFlux, TRMM-PR precipitation, and SSM/I surface winds. The differences between summer 1998 and the average of 2000 and 2001 are given. We infer that the warmer and saltier water in 1998 was due to a stronger warming effect than that in other years. Monthly mean net heat obtained in summer 1998 is greater by 15–30 W m^{-2} than those of other years. Downward Ekman pumping associated with a negative curl of wind stress also favors the vertical movement of warm surface water. On the other hand, the precipitation in summer 2000 and 2001 are much greater than that by 100–200 mm/month in 1998, and the precipitation was comparable to the surface water freshening in those years. Stronger surface winds in 2000 and 2001 facilitate vertical mixing of the surface low-salinity water. Therefore, significant interannual changes in the water masses of the upper ocean result mainly from the local air-sea forcing above.

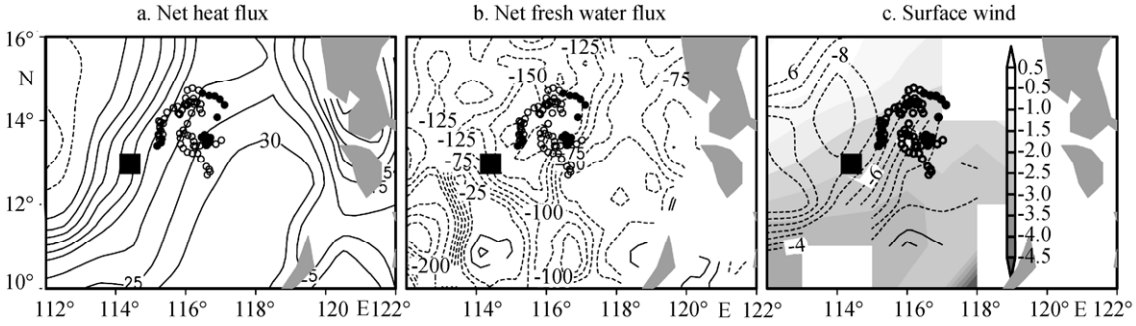

Fig.4 Difference in surface winds, net heat flux and precipitation between summer 1998 and the average of 2000/2001. Summer is defined as from June to August

Owing to the lack of observations, we could not analyze the cases of May and June in 2000 using in-situ data. Having known from WOA05 data, upper ocean is the warmest in May and June. With the help of the monthly Advanced Very High Resolution Radiometer (AVHRR) temperature, we found that the temperature in May and June of 2000 was much cooler than that in 2001 (figure not shown). In other words, the absence of observations in May and June of 2000 could not alter our findings of the cooling trend during 1998–2001. In addition, difference in surface winds and fluxes indicates more freshwater in summer 2000 than in 2001 (figure not shown). Therefore, the upper ocean was occupied by less-saline water in 2000 than in other years, suggesting that the absence of observations in May and June of 2000 did not affect the result of the decreasing trend of sea water salinity.

4 INTRASEASONAL VARIABILITY

4.1 Harmonic analysis

Besides robust seasonal and year-to-year changes in this region, significant intraseasonal variability has been recognized. We selected and compare one-year measurement of Argo_29018 from 3 August, 2000 to 26 July, 2001 with those of Buoy_SCS3.

By employing harmonic analysis, we studied the major oscillations of temperature and salinity in the upper ocean, and calculated $F_k=(C_k^2/2)/(2(s^2-C_k^2/2)/(n\text{-}2\text{-}1))$ to see if the k^{th} harmonic wave is significant, where k is the harmonic wave number, C_k the amplitude of the k^{th} harmonic wave, s^2 the variance of the time series, n number of the total sample, and F_k the F-distribution whose degrees of freedom vary between 2 and n-2-1. The period of the k^{th} harmonic wave is $365/k$ for daily mean Buoy_SCS3 data or $7\times52/k$ for weekly mean Argo_29018 data. Therefore, the first and second harmonic waves are annual and semi-annual variations, and the forth to fourteenth (26–91-day) waves are classified as intraseasonal variabilities. Table of F test shows the confidence levels are 3.11 and 3.18 for Buoy_SCS3 and Argo_29018, respectively. As the calculated F_k is greater than these values, the k^{th} harmonic wave is significant (dotted areas in Fig.5); insignificant

waves are marked by black lines.

As shown in Fig.5, the annual and semiannual cycles are the major periods, as for other variables in the SCS (Wang et al., 1997). Shaded areas indicate that the intraseasonal variability in the upper ocean is very strong. A significant intraseasonal variability in temperature was noticed in 25 and 50 m depth according to Buoy_SCS3 and Argo_29018 data, respectively. The 4^{th}–12^{th} (30–90-day) harmonic waves in temperature are significant for Buoy_SCS3. However, only the 5^{th}–9^{th} (40–75-day) harmonic waves are significant in Argo_29018 data. Different from the case for low-frequency signals, intraseasonal signals of Argo_29018 located at deeper levels than those of Buoy_SCS3, especially the 9^{th}-11^{th} waves in the time scale of 30–40 days, situated below 150 m.

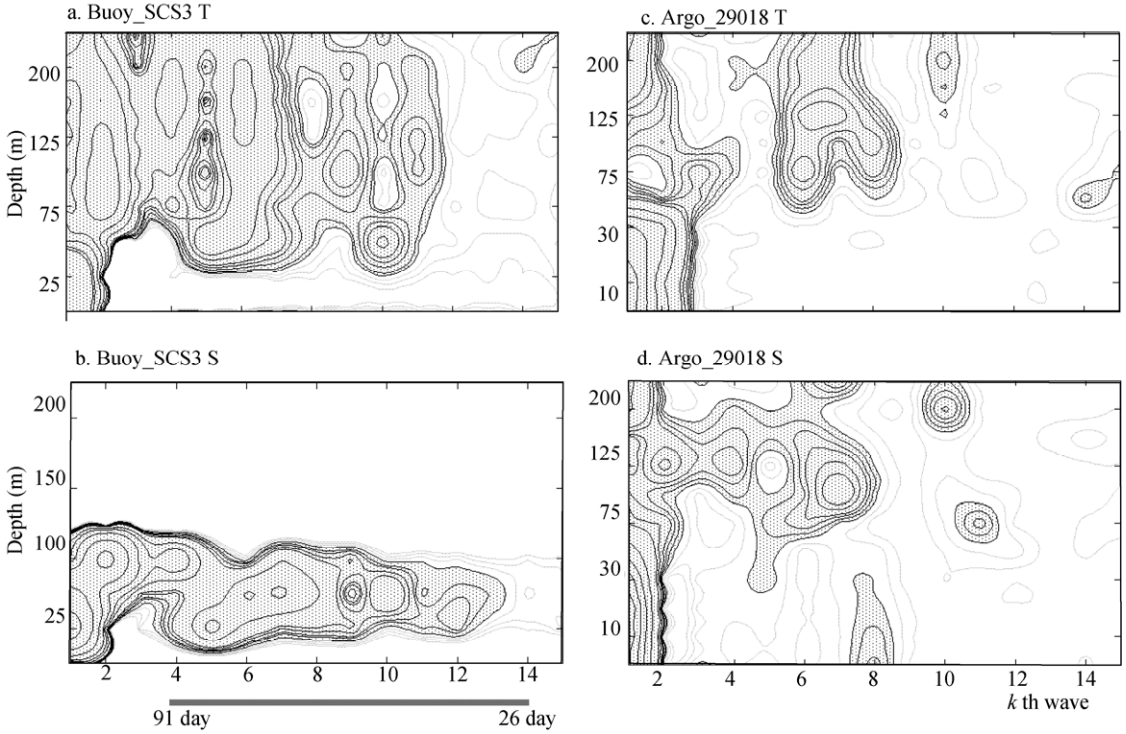

Fig.5 Harmonic analysis of vertical temperature and salinity recorded by SCSMEX Buoy_SCS3 (a, b) and Argo_29018 (c, d). The *X*-axis gives the k^{th} wave (*k*, 1–15) and the *Y*-axis the corresponding vertical depths. Dotted areas are statistically significant at 95% confidence level of *F* test. The band of 26–91days is indicated by a black bar below the wave numbers

Strong intraseasonal variability was also indicated by salinity data of both Buoy_SCS3 and Argo_29018. Almost all intraseasonal signals of Buoy_SCS3 in the upper 100 m have higher confidence levels. As shown in Fig.5d, intraseasonal salinity variation detected by Argo floats during 2000/2001 is much weaker than that detected by Buoy_SCS3. Similarly in temperature profiles, significant intraseasonal signals of salinity of Argo_29018 at the deeper levels are also shown, except for the 8^{th} harmonic wave. The Argo float data below 100 m recorded also remarkable intraseasonal variations. For example, intraseasonal salinity signals in scale of 35–90 days (4^{th}–8^{th} and 10^{th} harmonic waves) appears mainly below 100 m.

For more detail, we studied the intraseasonal anomalies of temperature and salinity separately using a 30–90-day band-pass filter. Such a filter is commonly used in intraseasonal variation studies and appropriate for studying the SCS. As shown in Fig.6, the axis of the maximum intraseasonal temperature and salinity signals are located mainly at the thermocline. Most significant intraseasonal temperature signals are between 25 and 150 m, typically amplitude is about 2°C. The strongest intraseasonal events recorded by Buoy_SCS3 are around May 26 to July 10, 1998 (a period of 45 days) and January 1 to March 2, 1999 (a period of 60 days). A typical intraseasonal fluctuation during 2000–2002 is from April 5 to May 24, 2001 (a period of 50 days), at an amplitude of about 2.5°C. In salinity, significant intraseasonal variability was confined above 150 m. The strongest variation measured by Buoy_SCS3 is from December 17, 1998 to February 15, 1999 (in 60 days), with an amplitude of 0.5. During the observational period of

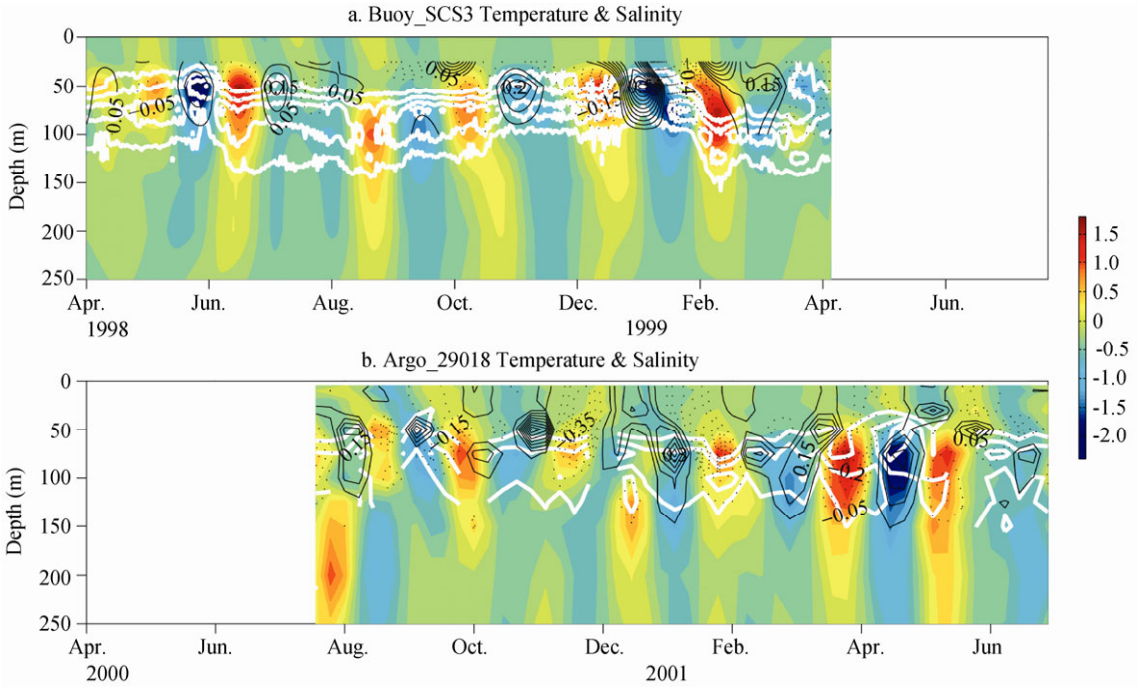

Fig.6 Time-depth sections of the intraseasonal temperature (shading) and salinity (contour) anomaly with the gradient of temperature greater than 0.08°C/m (white lines), based on (a) SCSMEX Buoy_SCS3, and (b) Argo_29018 data

Argo_29018, the variation is relatively small at <0.3 in 35 days. In addition, significant differences in intraseasonal temperature and salinity signals recorded by Argo_29018 took place at deeper depth mainly.

4.2 Effect of intraseasonally changing variable

We saw significant intraseasonal variations in the upper ocean from the fluctuation of mixed-layer depth. Turbulent mixing powered by surface winds, heat flux, and fresh water flux at air-sea interface create neutral buoyancy and a well-mixed column in the upper ocean. To explain the forcing mechanism that governs the variability of the mixed-layer depth, time series of the intraseasonal wind speed, net heat flux, and precipitation in Fig.7. All the time series show strong intraseasonal variability from 1998 to 2001.

In winter when northeast monsoon fully develops, surface winds and the surface heat status (warming and cooling) work together to generate a strong intraseasonal fluctuation in this region. For example, change in net heat flux corresponds well with variation in mixed-layer depth in winter. Strong wind bursts and surface cooling anomaly induces a relatively deep mixed layer. On the other hand, weak winds and warming signals are responsible for a thin surface mixed layer.

As the winter monsoon fades, surface heat flux becomes positive and the intraseasonal signal reaches its minimum in summer, the transition season of the monsoon. Weak winds in summer 1998 controlled was by a strong El Niño event; surface fresh water flux controlled and led to the strongest intraseasonal event in the measurement period of Buoy_SCS3. Sufficient precipitation contributed to the thinner mixed layer; and the following negative precipitation anomalies caused a deeper mixed layer. In September 2000, the fluctuation in the mixed layer was caused mainly by prevailing moderate winds and precipitation. More freshwater and a weaker wind forcing would bump up the mixed layer, or vice versa, deepen it.

The variability of the upper ocean is controlled by many processes, such as advection, mixing across the base of the mixed layer, propagating waves, and eddy fields. To investigate the relative importance of air-sea fluxes and advection or vertical mixing entrainment effect to the intraseasonal upper ocean variabilities, we studied the mixed-layer heat and freshwater balances. Without the estimates of advection or mixing across the base of the mixed layer, following Parampil et al. (2010): the amplitude of the response is measured by R, the ratio of root mean square, $R=RMS(\rho C_p H_0 \partial SST/\partial t)/RMS(Q_{eff})$. If $\partial SST/\partial t$ is entirely forced by Q_{eff}, $R = 1$. If $R > 1$ or $R < 1$, the advection or entrainment would be in phase with atmospheric forcing to increase or decrease the SST. For mixed-layer fresh water balance, the amplitude

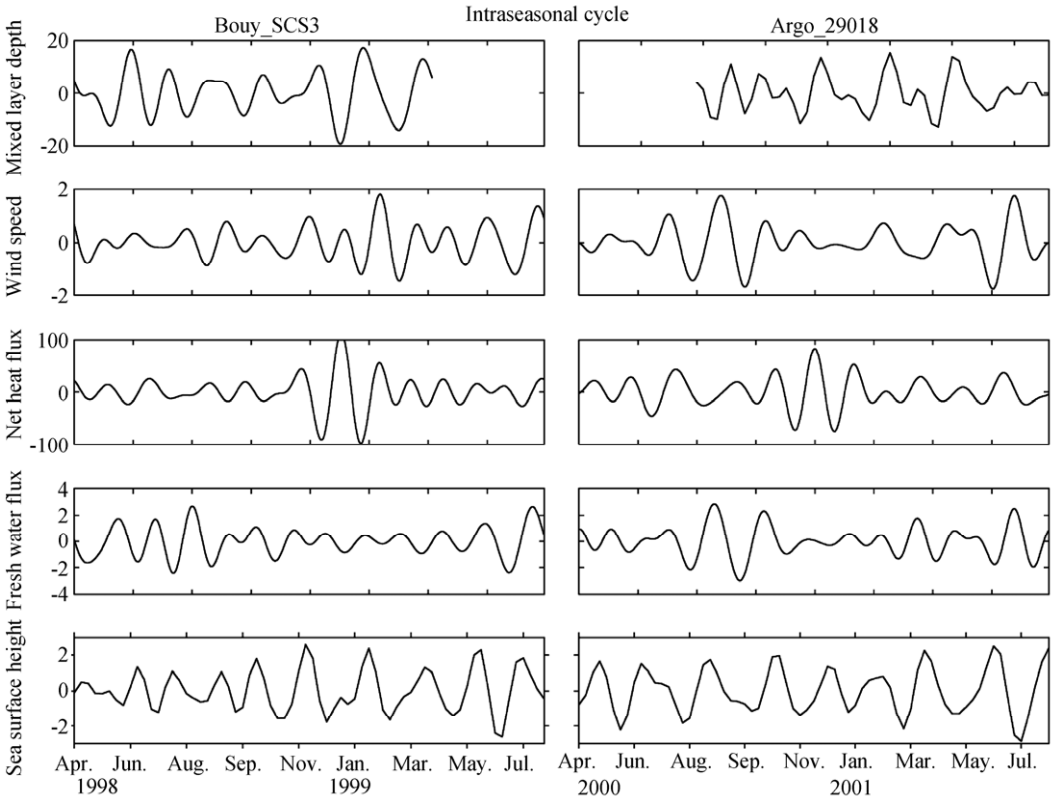

Fig.7 Time variations of the intraseasonal mixed-layer depth, wind speed, net heat flux, net fresh water, and sea surface height anomaly, recorded by SCSMEX Buoy_SCS3 (left) and Argo_29018 (right)

response is $R=RMS(\partial FW/\partial t)/RMS(P-E)$. Owing to the limitations of the vertical observation of Buoy_SCS3, the balance analysis was done for Argo_29018 data only.

Intraseasonal variability of the *SST* and $\partial SST/\partial t$ recorded by Argo_29018 (Fig.8a) is substantial. Comparison between the *SST* and $\partial SST/\partial t$ suggests that the phase and amplitude of the ocean response matches that of the forcing. In a particular situation, the amplitude of the ocean response is weaker in the case of rather stronger forcing. The amplitude response of intraseasonal oscillations is 0.70. Both warming and cooling of the upper ocean is weakly related to the forcing, especially in autumn and winter of 2000. Advection is the likely reason for somewhat muted response of the ocean to forcing since no evidence of sustained mixing across the base of the mixed layer. The rate of the intraseasonal variability of the freshwater change is often less than that of the surface flux (Fig.8b). The amplitude response of the intraseasonal variability of the mixed-layer fresh water content is 0.38, showing that in general, surface flux does not determine freshwater variability even in a monsoon season, and lateral salinity advection probably plays a dominant role.

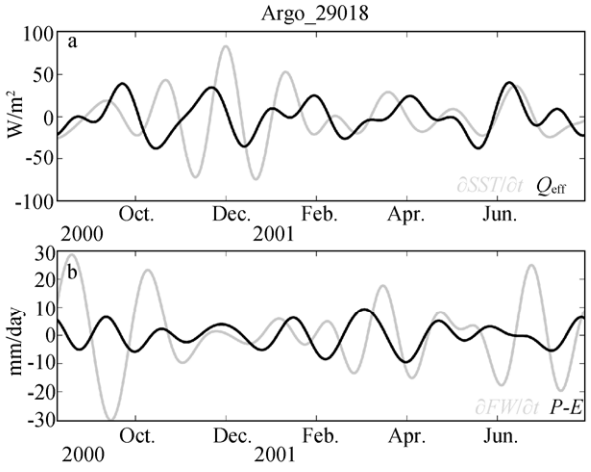

Fig.8 (a) Intraseasonal mixed-layer temperature change (gray) and net heat flux (black) and (b) the rate of change of the freshwater (gray) and net fresh water flux (*P–E*) (black) recorded by Argo_29018

5 DISCUSSION

In addition, some other issues remain unresolved. For example, intraseasonal variations in temperature and salinity in deeper waters 2000–2002 have not been well explained. Is this phenomenon real or as a result of just by errors in Argo float measurements?

In the significant events described earlier in

previous sections, air-sea forcings including surface winds, net fresh water flux, and heat flux, work together and lead to a strong intraseasonal variation in the upper ocean. However, a strong intraseasonal event in 2001 cannot be explained by local air-sea forcings. The intraseasonal signals of surface winds, surface heating/cooling and fresh water flux are very weak.

As we know, the SCS has energetic mesoscale variability additional to distinct seasonal cycle, particularly in winter (Xiu et al., 2010). Observations and eddy-resolving numerical models all show two bands of active mesoscale variability propagation in the north of 10°N in the SCS. One lies along the northwestern boundary west of Luzon Strait and the other is across the central basin, steered by the bathymetry (Wang et al., 2000; Zhuang et al., 2010). In recent years, satellite altimetry has advanced the study of mesoscale variability propagation in the SCS. The active mesoscale variability might have an impact on the strong intraseasonal variability in the region we investigated. Basically, the intraseasonal sea surface height anomaly and other the air-sea parameters (Fig.7) are obvious throughout a year. Although the mesoscale eddy propagation is likely related to the variation, the specific processes remain unknown. The impact of energetic mesoscale propagation radiated from the east boundary on the intraseasonal variability in the region, and the specific effect of the active eddy propagation on the intraseasonal fluctuations needs further study and discussion. On the other hand, our study discusses only the possible effect of advection or vertical mixing using a simple method. Further examination on the mixed-layer heat and fresh water balance requires more observations.

6 SUMMARY

In this paper, the interannual and intraseasonal variations of the water masses in the upper ocean in the central SCS are studied using a long-lived Argo float and high-resolution ATLAS buoy observations. The T-S diagram indicates that the properties of the water mass have significantly changes from 1998 to 2002. Water in 2000, 2001 and 2002 was colder and fresher than that in 1998 by 1–1.7°C and 0.5–0.8, respectively. A detailed examination reveals that this remarkable difference is mainly due to a change in summer. Large differences in net heat flux and precipitation suggest that warmer and saltier waters in 1998 result mainly from extra forcing by the atmosphere.

Besides robust seasonal and year-to-year changes, significant intraseasonal variability in the upper ocean was also revealed. Band-pass filter and harmonic analysis shows that the maximum temperature and salinity fluctuations are roughly located on the thermocline. Significant intraseasonal temperature signals falls mainly 25–150 m with typical amplitude and period at ~2°C and 40–60 days, respectively. However, the intraseasonal variability of salinity is confined above 150 m, with a typical period and amplitude at 35–60 days and 0.3–0.5, respectively. The intraseasonal variation in salinity during 2000–2001 was much smaller than that during 1998–1999, as observed by Argo floats and Buoy_SCS3.

Compared with surface winds, the net heat flux and precipitation strongly affect the intraseasonal fluctuation. Change in net heat flux corresponds to the major variability in the mixed layer depth in winter in 1999–2000. In summer 1998, surface heat and precipitation together resulted in the largest intraseasonal variation in the mixed layer. In September 2000, the fluctuation mainly attribute to changes in surface winds and precipitation. The mesoscale variability is thought to be important to the strong intraseasonal variability. In the large-variation events described above, active mesoscale eddy propagation and other air-sea forcings together caused strong intraseasonal fluctuations. However, strong intraseasonal variation in 2001 might be attributed to active wave propagation from the eastern boundary rather than the local air-sea interaction. The intraseasonal mixed-layer heat and freshwater balance at Argo_29018 shows that the amplitude of the ocean response is usually weaker even under a much stronger forcing. Advection is the likely reason for somewhat muted response of the ocean to forcing.

7 ACKNOWLEDGEMENT

Data were collected and made freely available by the International Argo Project and the national programs that contribute to it (http://www.argo.ucsd.edu, http://argo.jcommops.org, accessible on 2010/4/10). Sincere thanks are extended to the Data Center of the SCSMEX Project. Thanks are also extended to three anonymous reviewers for their valuable comments on the manuscript

References

Argo Science Team, 2000. Report of the Argo Science Team 2nd Meeting (AST-2) March 7–9, 2000, Southampton

Oceanography Centre, Southampton, U.K.

Argo Science Team, 2001. Argo: The global array of profiling floats. *In*: Koblinsky C J, Smith N R eds. Observing the Oceans in the 21st Century, GODAE Project Office, Bureau of Meteorology, Melbourne. p. 248–258

Argo Science Team, 2002. Report of the Argo Science Team 4th Meeting (AST-4) March 12–14, 2002, CSIRO Division of Marine Sciences, Hobart, Tasmania, Australia.

Holte J, Talley L. 2009. A New Algorithm for Finding Mixed Layer Depths with Applications to Argo Data and Subantarctic Mode Water Formation. *Journal of Atmospheric and Oceanic Technology*, **26**: 1 920-1 939.

Huffman G J, Adler R F, Bolvin D T et al. 2007. The TRMM multi-satellite precipitation analysis: quasi-global, multi-year, combined-sensor precipitation estimates at fine scale. *J. Hydrometeorol*., **8(1)**: 38-55.

Liu Q Y, Yang H J, Wang Q. 2000. Dynamic characteristics of seasonal thermocline in the deep sea region of the South China Sea. *Chin. J. Oceanol. Limnol*., **18**: 104-109.

Liu Q Y, Jia Y L, Liu P H et al. 2001. Seasonal and intraseasonal thermocline variability in the central South China Sea. *Geophys. Res. Lett*., **28(23)**: 4 467-4 470.

Liu Z H, Xu J P, Zhu B K et al. 2007. The upper ocean response to tropical cyclones in northwestern Pacific analyzed with Argo data. *Chin. J. Oceanol. Limnol*., **25(2)**: 123-131.

Morel A. 1988. Optical modeling of the upper ocean in relation to its biogenous matter content (case I waters). *J. Geophys. Res*., **93**: 1 652-1 665.

Ohno Y, Kobayashi T, Iwasaka N et al. 2004. The mixed layer depth in the North Pacific as detected by the Argo floats. *Geophys. Res. Lett*., **31**: L11306, doi:10.1029/2004GL019576.

Oka E, Suga T. 2003. Formation region of North Pacific subtropical mode water in the late winter of 2003. *Geophys. Res. Lett*., **30(23)**: 2205, doi: 10.1029/2003GL018581.

Oka E. 2005. Long-term Sensor Drift Found in Recovered Argo Profiling Floats. *Journal of Oceanography*, **61**: 775-781.

Parampil S R, Gera A, Ravichandran M et al. 2010 Intraseasonal response of mixed layer temperature and salinity in the Bay of Bengal to heat and freshwater flux. *J. Geophys. Res*., **115**, C05002, doi: 10.1029/2009JC005790.

Qu T, Meyers G. 2005. Seasonal variation of barrier layer in the southeastern tropical Indian Ocean. *J. Geophys. Res*. **110**: doi: C11003, 10.1029/2004JC002816.

Sato K, Suga T, Hanawa K. 2004. Barrier layer in the North Pacific subtropical gyre. *Geophys. Res. Lett*., **31**: L05301, doi: 10.1029/2003GL018590.

Su Z J, Wang D, Zhang R H et al. 2008. Preliminary results of the Argo floats in the South China Sea. *Oceanologia et Limnologia Sinica*, **39 (2)**: 97-104. (in Chinese with English abstract)

Su Z J, Wang D, Zhang R H. et al. 2008. Preliminary results of the Argo floats in the South China Sea. *Oceanologia et Limnologia Sinica*, **39 (2)**: 97-104. (in Chinese with English abstract)

Volkov D L, Larnicol G, Dorandeu J. 2007. Improving the quality of satellite altimetry data over continental shelves. *J. Geophys. Res*., **112**, C06020, doi: 10.1029/2006JC003765.

Wang D, Zhou F X, Li Y P. 1997. Characteristics of sea surface temperature and surface heat budget on annual cycle time scales in the South China Sea. *Acta Oceanol. Sinica*, **15**: 111-125

Wang L P, Koblinsky C J, Howden S. 2000. Mesoscale variability in the South China Sea from the TOPEX/Poseidon altimetry data. *Deep Sea Res*, *Part I*, **47**: 681-708.

Wentz F J. 1997. A well-calibrated ocean algorithm for SSM/I. *J. Geophys. Res*., **102**: 8 703-8 718.

Wong A P S, Johnson G C. 2003. South Pacific eastern subtropical mode water. *J. Phys. Oceanogr*., **33**: 1 493-1 509.

Xie Q, Wu X Y, Yuan W Y et al. 2007a. Life cycle of intraseasonal oscillation of summer SST in the western South China Sea. *Acta Oceanol. Sinica*, **3**: 1-8.

Xie S P, Chang C H, Xie Q et al. 2007b. Intraseasonal variability in the summer South China Sea: wind jet, cold filament, and recirculations. *J. Geophys. Res*., **112**: C10008, doi: 10.1029/2007JC004238

Xiu P, Chai F, Shi L et al. 2010. A census of eddy activities in the South China Sea during 1993-2007. *J. Geophys. Res*., **115**, C03012, doi:10.1029/2009JC005657.

Xue H, Chai F, Pettigrew N et al. 2004. Kuroshio intrusion and the circulation in the South China Sea. *J. Geophys. Res*., **109**: C02017, doi:10.1029/2002JC001724.

Yu L S, Weller R A. 2007. Objectively analyzed air-sea heat fluxes for the global ice-free ocean (1981–2005). *Bull. Am. Meteorol. Soc*., **88**: 527-539.

Zeng L L, Shi P, Wang D et al. 2009a. Seasonal and interannual variabilities of evaporation and net fresh water flux in the South China Sea. *Chinese J. Geophys*., **52(4)**: 929-938. (in Chinese with English abstract)

Zeng L L, Du Y, Xie S P et al. 2009b. Barrier layer in the South China Sea during summer 2000. *Dynamics of Atmospheres and Oceans*, **47(1-3)**: 38-54, doi: 10.1016/j.dynatmoce.2008.08.001

Zhuang W, Xie S P, Wang D et al. 2010. Intraseasonal variability in sea surface height over the South China Sea. *J. Geophys. Res*., **115**, C04010, doi: 10.1029/2009JC005647.